JACS
JOURNAL OF THE AMERICAN CHEMICAL SOCIETY
Article
pubs.acs.org/JACS

TiO_2–ZnS Cascade Electron Transport Layer for Efficient Formamidinium Tin Iodide Perovskite Solar Cells

Weijun Ke,[†] Constantinos C. Stoumpos,[†] Jenna Leigh Logsdon,[†] Michael R. Wasielewski,[†] Yanfa Yan,[§] Guojia Fang,[‡] and Mercouri G. Kanatzidis*[,†]

[†]Department of Chemistry, Northwestern University, Evanston, Illinois 60208, United States

[‡]Key Laboratory of Artificial Micro- and Nano-structures of Ministry of Education of China, School of Physics and Technology, Wuhan University, Wuhan 430072, China

[§]Department of Physics and Astronomy and Wright Center for Photovoltaics Innovation and Commercialization, The University of Toledo, Toledo, Ohio 43606, United States

Supporting Information

ABSTRACT: Achieving high open-circuit voltage (V_{oc}) for tin-based perovskite solar cells is challenging. Here, we demonstrate that a ZnS interfacial layer can improve the V_{oc} and photovoltaic performance of formamidinium tin iodide ($FASnI_3$) perovskite solar cells. The TiO_2–ZnS electron transporting layer (ETL) with cascade conduction band structure can effectively reduce the interfacial charge recombination and facilitate electron transfer. Our best-performing $FASnI_3$ perovskite solar cell using the cascaded TiO_2–ZnS ETL has achieved a power conversion efficiency of 5.27%, with a higher V_{oc} of 0.380 V, a short-circuit current density of 23.09 mA cm^{-2}, and a fill factor of 60.01%. The cascade structure is further validated with a TiO_2–CdS ETL. Our results suggest a new approach for further improving the performance of tin-based perovskite solar cells with a higher V_{oc}.

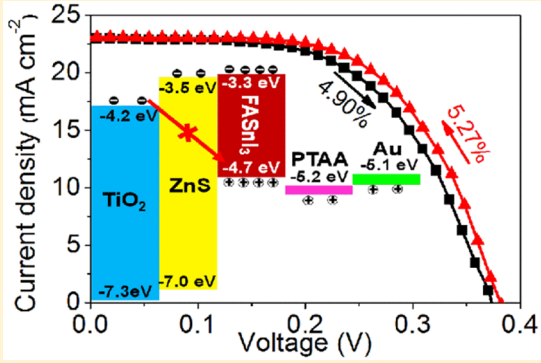

INTRODUCTION

Organic–inorganic hybrid halide perovskite materials have drawn enormous research interest in the past few years, mostly due to their superior photovoltaic properties, such as extremely high optical absorption coefficients, tunable band gaps, high electron and hole mobilities, and long carrier lifetimes.[1−4] A certified power conversion efficiency (PCE) of 22.1% has been achieved;[5] the most efficient cells are, however, still based on methylammonium (MA) or formamidinium (FA) lead iodide as light-absorbing material. The toxicity of Pb undoubtedly hinders the commercialization of this new technology, thus driving the scientific community to seek a less toxic replacement. The possible candidates enabling the perovskite structure formation are Cu, Ge, Sn, Sb, and Bi,[6,7] of which Sn-based perovskites are particularly good candidates since both Pb and Sn belong to group 14 of the periodic table and possess similar optical and electrical characteristics.[8−10] Over the past 3 years, a few groups have successfully fabricated lead-free Sn-based perovskite solar cells using both regular and inverted device structures.[11−18] Since Sn-based perovskites have lower optical band gap (E_g) than their Pb-based analogues, their devices thus generally produce higher short-circuit current densities (J_{sc}), another factor that makes them attractive for solar cell applications.[8] Yet the overall performance of Sn-based devices is still low, mainly hampered by the moderate fill factor (FF) (low film quality), poor open-circuit voltage (V_{oc}) (interfacial barrier and imperfect device structure), and poor reproducibility. Recently, Seok and co-workers reported efficient and stable formamidinium tin iodide ($FASnI_3$) perovskite solar cells in which they used a SnF_2–pyrazine complex to improve the perovskite film morphology and achieved a promising FF of 63% and a PCE of 4.8%.[19] However, the reported V_{oc} of 0.32 V was still relatively low, considering the E_g of $FASnI_3$ is 1.40 eV. Similarly low V_{oc} has also been reported in other Sn-based solar cells. In principle, the theoretical maximum of V_{oc} in solar cells is determined by the bandgap of $FASnI_3$ after accounting for the voltage losses arising from radiative and non-radiative recombination processes. According to this scheme, V_{oc} should be approximately 1 V, but due to the tendency of Sn^{2+} to self-dope by partial oxidation to Sn^{4+}, the V_{oc} in Sn-based perovskites is typically significantly lower. Therefore, solving the V_{oc} loss is a critical step in bringing the photovoltaic performance of Sn-based perovskite solar cells closer to their theoretical limit. Given that V_{oc} is defined by the energy difference between TiO_2's conduction band minimum (CBM) and the perovskite's valence band maximum (VBM), one possible reason for the low V_{oc} could be the shallow VBM of the Sn-based perovskites, which may limit the V_{oc} output.[17]

Received: August 22, 2016
Published: October 25, 2016

DOI: 10.1021/jacs.6b08790
J. Am. Chem. Soc. 2016, 138, 14998−15003

Another possibility is that carrier recombination between electrons in TiO_2 and holes in Sn-perovskites may lower the quasi-Fermi level of the electrons. This process is more severe in the Sn-based perovskites than the Pb-based ones because Sn-perovskites possess higher background hole carrier densities, stemming from the facile oxidization of Sn^{2+} to Sn^{4+}. Therefore, a V_{oc} improvement in Sn-based perovskite solar cells is expected if the recombination process can be suppressed. With these considerations in mind, we set out to study a cascade ETL structure for $FASnI_3$ solar cells by growing ZnS onto TiO_2. First, ZnS is an *n*-type semiconductor with a wide E_g of 3.5−3.8 eV.[20,21] It has higher electron mobility than TiO_2, potentially improving electron extraction and transfer. It has been reported to serve as an ETL for organic solar cells and interfacial passivation layer for quantum-dot-sensitized solar cells.[20−23] Second, the CBM of $FASnI_3$ is closer to that of ZnS than TiO_2, so cascading electrons move from $FASnI_3$ to ZnS and then TiO_2. Third, the presence of the thin ZnS layer acts as an energy barrier, inhibiting charge recombination between TiO_2 and $FASnI_3$. The relaxation of the photogenerated electrons is much fast than the carrier recombination at interfaces. Because the CBM of ZnS is higher in energy than the CBM of TiO_2, electrons relaxed to TiO_2 will be inhibited to recombine with holes in the $FASnI_3$ absorber at the interface.

In this paper, we show that coating TiO_2 with ZnS is an effective approach to facilitate electron extraction from $FASnI_3$ into TiO_2. As a result, the ZnS-coated TiO_2 device outperforms the neat TiO_2 one in V_{oc} (380 vs 270 mV) while maintaining comparable J_{sc} and FF, essentially yielding a PCE of 5.27%. Photoluminescence (PL), time-resolved photoluminescence (TRPL), and electrochemical impedance spectroscopy (EIS) measurements confirm that devices employing the ZnS interface layer have a more efficient electron transfer pathway and lower interfacial recombination compared to those without ZnS. Our studies demonstrate that turning the ETL into an energy cascade structure is a viable approach to boost the V_{oc} and efficiency of lead-free tin-based perovskite solar cells.

EXPERIMENTAL SECTION

Device Fabrication. The process of preparing compact and mesoporous TiO_2 layers on FTO has been reported elsewhere.[17,24] First, a compact TiO_2 layer was spin-coated onto FTO substrate (Tec15, Hartford Glass) from ethanol solution of titanium isopropoxide at 2000 rpm for 30 s and then annealed in air at 500 °C for 20 min. Subsequently, a mesoporous TiO_2 layer composed of 20 nm particles (Dyesol DSL 18NR-T) was spin-coated onto the compact layer using a diluted solution in anhydrous ethanol (1:3.5 weight ratio) at 500 rpm for 1 min and then annealed in air at 500 °C for 15 min. Finally, the annealed mesoporous TiO_2 film was dipped into a 0.02 M aqueous $TiCl_4$ solution at 70 °C for 30 min and then annealed at 500 °C for 15 min. The ZnS and CdS films were synthesized by using a SILAR method based on a method reported in the literature;[23] the mesoporous TiO_2 film was alternately dipped into 0.1 M $Zn(NO_3)_2$ or $Cd(NO_3)_2$ solution in ethanol, 0.1 M Na_2S solution in methanol, and deionized water with a volume ratio of 1:3. This SILAR process was repeated two times.

The solvent-engineering method for preparing the $FASnI_3$ perovskite film deposited on mesoporous layer is similar to the method reported in the literature.[25] The precursor solution, consisting of 372.5 mg of homemade SnI_2, 172 mg of FAI (Dyesol), and 31.4 mg of SnF_2 (sigma, 99%) dissolved in 723 μL of *N*,*N*-dimethylformamide and 81 μL of dimethyl sulfoxide, was spin-coated on the mesoporous layer with a spin rate of 3000 rpm for 60 s. The SnI_2 synthesis was described in our previous work.[17] First, 300 μL of diethyl ether was dropped on the spinning substrate during the spin-coating process. The substrate was then annealed at 70 °C for 10 min on a hot plate. For the one-step method, the precursor and film deposition methods are similar, except for the use of diethyl ether anti-solvent. The solution of hole transporting material (HTM), consisting of 32 mg of poly[bis(4-phenyl)(2,4,6-trimethylphenyl)amine] (PTAA, Sigma-Aldrich, 99%) and 3.6 mg of 4-isopropyl-4′-methyldiphenyliodonium tetrakis(pentafluorophenyl)borate (TPFB, TCI America) in 1.6 mL of chlorobenzene, was spin-coated on the $FASnI_3$ perovskite film at 1500 rpm for 30 s and then annealed at 70 °C for 5 min.[17] All these procedures were performed in a N_2 glovebox. To complete the device, a 100 nm thick Au electrode was thermally evaporated on top of the HTM layer. During the evaporation process, the sample was inevitably exposed to air for about 10 min. The active area of the solar cells was 0.15−0.18 cm^2, defined by the overlapping area between the un-etched FTO glass and Au electrode.

Film and Device Characterization. X-ray diffraction (XRD) spectra of the $FASnI_3$ perovskite films were obtained on a CPS 120 INEL X-ray diffractometer with a Cu Kα radiation source operating at 40 kV and 20 mA. The morphology of the devices and films was characterized by high-resolution field emission scanning electron microscopy (SEM, Hitachi SU8030). Ultraviolet−visible (UV−vis) and absorbance spectra of the $FASnI_3$ perovskite films were obtained by using a Shimadzu UV-3600 PC double-beam, double-monochromator spectrophotometer. X-ray photoelectron spectroscopy (XPS) was performed on a Thermo Scientific ESCALAB 250Xi system. The external quantum efficiency (EQE) spectrum was characterized by an Oriel model QE-PV-SI instrument equipped with a NIST-certified Si diode. Photocurrent density−voltage (*J*−*V*) curves were characterized by a Keithley model 2400 instrument under AM1.5G simulated irradiation with a standard solar simulator (Abet Technologies). The light intensity of the solar simulator was calibrated by a NREL-certified monocrystalline silicon solar cell. EIS measurements are performed on a CHI electrochemical workstation. The energy of the valence band of the $FASnI_3$ films was measured by using photoemission spectroscopy in air (PESA, AC-2, Riken Keiki). The $FASnI_3$ films were grown on mesoporous TiO_2 and measured right after being exposed to air to minimize the oxidization of the films. TRPL lifetimes were measured with a streak camera setup (Hamamatsu C4334 Streakscope). The instrument response function (IRF) was approximately 2% of the sweep window. A commercial direct diode-pumped 100 kHz amplifier (Spirit 1040-4, Spectra Physics) produces a fundamental beam of 1040 nm (350 fs, 4.5 W). This light was used to pump a non-collinear optical parametric amplifier (Spirit-NOPA, Spectra-Physics) which delivers high repetition rate pulses. The samples were excited with 525 nm, 0.1 nJ pulses.

RESULTS AND DISCUSSION

The device structure of $FASnI_3$ solar cells used in this study is shown in Figure 1a. Compact TiO_2, mesoporous TiO_2, and ZnS were grown on FTO as the ETL. $FASnI_3$ perovskite films were coated on the ETL. PTAA and evaporated gold film were used as HTM and back metal electrode, respectively. The

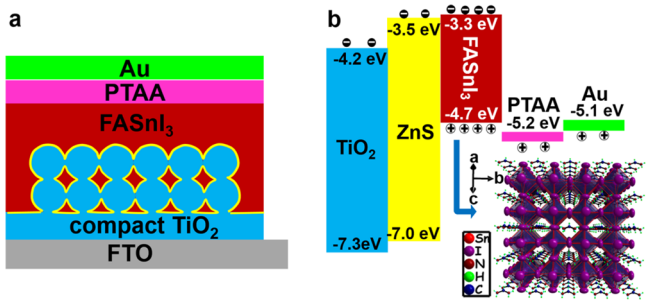

Figure 1. Schematic view of (a) the device structure and (b) the energy band diagram of the $FASnI_3$ solar cells and crystal structure of the perovskite absorber.

DOI: 10.1021/jacs.6b08790
J. Am. Chem. Soc. 2016, 138, 14998−15003

energy band diagram is shown in Figure 1b, in which the E_g of the tetragonal crystalline films of $FASnI_3$ is 1.4 eV,[8] and the VBM is ∼−4.7 eV. These energies were estimated from the Tauc plot of the absorption spectrum (Figure S1) and photoemission spectroscopy in air (Figure S2), respectively. The CBM of the $FASnI_3$ film is estimated to be ∼−3.3 eV by subtracting E_g from the VBM. Since the CBM of ZnS (∼−3.5 eV)[20,21] is between those of $FASnI_3$ and TiO_2 (∼−4.2 eV), photoexcited electrons in the CB of $FASnI_3$ cascade into TiO_2 via ZnS. Simultaneously, the energy barrier at the TiO_2/ZnS interface would effectively block charge recombination, which should essentially increase the quasi-Fermi level for electrons and raise the V_{oc} value. We note that the CBM of TiO_2 (∼−4.2 eV) is much lower than that of $FASnI_3$, thus limiting the output V_{oc}. Nevertheless, we certainly expect V_{oc} enhancement by suppressing the recombination at the TiO_2/$FASnI_3$ interface, since $FASnI_3$ has a rather high background hole carrier density, and thus the recombination would be significant if the $FASnI_3$ films have a direct contact with TiO_2. The VBM of $FASnI_3$ is slightly higher than that of the PTAA, potentially posing a barrier for hole carrier transporting. However, the $FASnI_3$ film is briefly exposed to air during device fabrication, given the nature of our current experimental setup, and as a result, the surface of the perovskite films is *p*-doped, producing an ohmic contact with the PTAA layer.[8,17] Therefore, even though an energy barrier exists between the $FASnI_3$ and PTAA layers originally, hole carriers can still be effectively transferred.

We first studied film morphology by using SEM. Figure 2a,b shows the comparison of neat TiO_2 and ZnS coated-TiO_2 (denoted as TiO_2−ZnS) mesoporous films; TiO_2−ZnS films were grown by using the successive ionic layer adsorption and reaction (SILAR) method.[23] The SEM images indicate that the addition of the ZnS layer does not alter the morphology of the underlying mesoporous TiO_2 layer, suggesting the formation of a very thin ZnS layer. The presence of ZnS was independently confirmed by XPS. Ti 2p, O 1s, Zn 2p, and S 2p peaks were all observed, as shown in the XPS spectra (Figure S3). The $FASnI_3$ films were prepared by a solvent-engineering method, analogous to the one reported for the fabrication of efficient Pb- and Sn-based perovskite films,[26−28] since the films made by the conventional one-step method showed poor surface coverage (Figure S4a).[19] Note that all the $FASnI_3$ perovskite films used in this study include 20% SnF_2 as an additive to reduce the background hole carrier density and improve the solar cell performance.[11,29] Figure 2c,d shows the surface morphology of the $FASnI_3$ perovskite films prepared by the solvent-engineering method on the neat TiO_2 and TiO_2−ZnS substrates, revealing uniform and high surface coverage for both substrates. Once again, coating TiO_2 with a very thin ZnS layer does not alter the film's overall morphology. During these experiments, we did not observe phase separation on the surface of the perovskite films caused by excess SnF_2, a phenomenon that has been reported elsewhere.[19] This is attributed to the use of diethyl ether as an anti-solvent in our fabrication procedure instead of the conventionally used chlorobenzene. In Figure S4b, it is obvious that the film prepared by an anti-solvent of chlorobenzene has worse film coverage. The uniform and pinhole-less perovskite films efficiently prevent the recombination caused by a direct contact between HTM and ETL, and thus allow us to systematically study the effect of the Zn interface layer on the device performance. A cross-sectional SEM image of a completed $FASnI_3$ perovskite solar cell employing mesoporous TiO_2−ZnS layer is shown in Figure 2e. A 500 nm-thick capping layer of the $FASnI_3$ is formed on top of a 700 nm-thick TiO_2−ZnS layer to allow optimal light-harvesting efficiency since Sn-based perovskites are known to have a lower absorption coefficient than Pb-based perovskites especially in the long wavelength range.

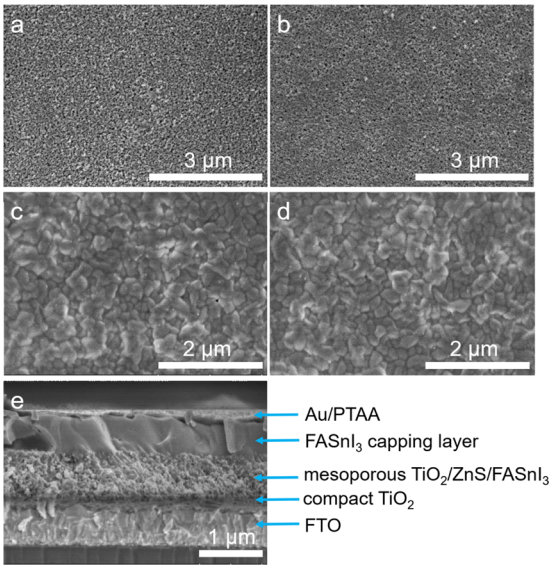

Figure 2. Top view SEM images of the mesoporous TiO_2 (a) without and (b) with ZnS-coated layer. Top view SEM images of a $FASnI_3$ film deposited on the mesoporous TiO_2 (c) without and (d) with ZnS-coated layer. (e) Cross-sectional SEM image of a completed device.

We further characterized our $FASnI_3$ films using UV−vis spectroscopy and XRD. The optical absorption spectra of $FASnI_3$ films on TiO_2 and on TiO_2−ZnS films are very similar, indicating that both film systems have similar composition and thickness. Moreover, the XRD patterns reveal an identical crystal growth habit for both substrates. As shown in Figure 3b, the $FASnI_3$ films formed on TiO_2 and ZnS both crystallize in orthorhombic structure (*Amm*2 space group) with no preferred orientation.[14,19] These results indicate that the ZnS interface layer does not affect the $FASnI_3$ film quality, namely thickness and crystallinity; thus, we can attribute the differences arising in the devices to the ZnS layer alone.

Having established the quality of our films, we then proceeded to the main focus of this work, which was to investigate the effect of the ZnS layer on the $FASnI_3$ solar cell performance. Figure 4a shows the *J*−*V* curves of two representative $FASnI_3$ perovskite solar cells, without and with a ZnS layer. The neat mesoporous TiO_2 device achieved a PCE of 3.69% with a V_{oc} of 0.290 V, a J_{sc} of 23.14 mA cm^{-2}, and a FF of 54.90% when measured under reverse voltage scanning (that is, from V_{oc} to 0 V). We observed a significant performance improvement in the ZnS-coated TiO_2, yielding a PCE of 4.72% with a V_{oc} of 0.366 V, a J_{sc} of 22.94 mA cm^{-2}, and a FF of 56.33% under the same measurement conditions. The photovoltaic parameters are summarized in Figure S5 and Table 1. It is clear that there is a significant enhancement in V_{oc}, while the J_{sc} values of the TiO_2−ZnS and the neat TiO_2 devices are comparable, implying that the ZnS layer does not hinder electron transfer from the $FASnI_3$ to ZnS. The slightly better FF also supports our initial hypothesis of a more efficient electron transfer process and the consequent suppression of the recombination. Additionally, we found that the thickness of

DOI: 10.1021/jacs.6b08790
J. Am. Chem. Soc. 2016, 138, 14998−15003

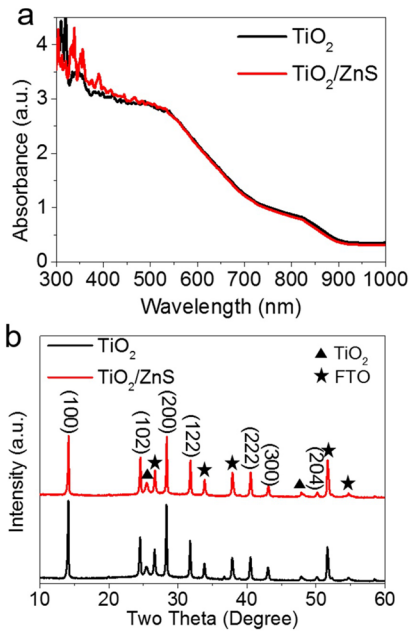

Figure 3. (a) UV−vis optical absorption spectra and (b) XRD patterns of $FASnI_3$ perovskite films grown on mesoporous TiO_2 and TiO_2−ZnS films. The *hkl* indices shown belong to the tetragonal perovskite structure of $FASnI_3$, corresponding to lattice parameters of 6.3286, 8.9554, and 8.9463.

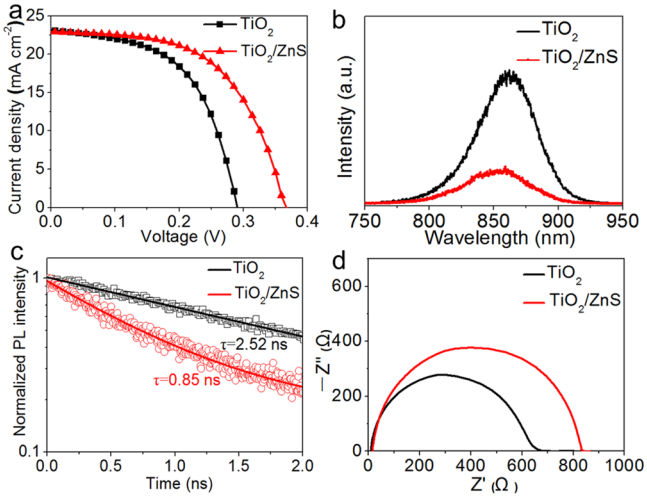

Figure 4. (a) J−V curves of the $FASnI_3$ perovskite solar cells using neat and ZnS-modified mesoporous TiO_2 measured under reverse voltage scanning. (b) PL spectra and (c) TRPL spectra of the $FASnI_3$ perovskite films coated on neat and ZnS-modified mesoporous TiO_2. (d) Nyquist plots of the $FASnI_3$ perovskite solar cells using neat and ZnS-modified mesoporous TiO_2 measured at 0 V bias in the dark.

Table 1. Summary of the Photovoltaic Parameters of the Solar Cells with Neat and ZnS-Modified Mesoporous TiO_2, Measured under Reverse Voltage Scanning[a]

ETL	V_{oc} [V]	J_{sc} [mA cm^{-2}]	FF [%]	PCE [%]
TiO_2	0.29 ± 0.02	22.89 ± 0.39	53.44 ± 1.42	3.59 ± 0.26
TiO_2/ZnS	0.37 ± 0.01	22.49 ± 0.41	56.74 ± 2.15	4.74 ± 0.25

[a]The photovoltaic parameters are the average of measurements using 10 devices.

ZnS is critical to the device performance, as demonstrated in Figure S6; the ZnS layer thickness was controlled by the number of the SILAR deposition cycles. In particular, when the ZnS is too thin, the V_{oc} drops (but it is still better than that of the neat devices), probably because the TiO_2 was not fully covered with the ZnS. On the other hand, when the ZnS becomes too thick, V_{oc} improves further, but at the same time J_{sc} drops. The best device performance was obtained from samples with two ZnS deposition SILAR cycles.

To further study the advantages that the ZnS interface layer brings to the electron transfer, we compared PL and TRPL spectra of the $FASnI_3$ perovskite films grown on TiO_2 with and without ZnS. Figure 4b shows the PL spectra of the perovskite films on different substrates, both displaying an emission peak at about 870 nm. Note that the PL intensity of the film deposited on the mesoporous TiO_2−ZnS layer is much lower than that of the film deposited on neat TiO_2 substrate. Since the two films exhibit very similar absorption bandwidths and peak maxima, the significantly reduced PL intensity can be attributed to the quenching effect (improved charge collection) caused by the better electron transfer promoted by the ZnS. The TRPL results of the $FASnI_3$ perovskite films deposited on TiO_2 with and without ZnS are shown in Figure 4c. The $FASnI_3$ perovskite film deposited on neat TiO_2 has an estimated carrier lifetime of 2.52 ns. In contrast, the carrier lifetime of the $FASnI_3$ perovskite film deposited on TiO_2−ZnS is ∼2.5 times shorter (τ = 0.85 ns), implying a faster electron transfer process.

To further validate that the TiO_2−ZnS cascade structure can, in fact, reduce the interfacial charge recombination, we performed EIS measurements on the $FASnI_3$ solar cells. Figure 4d shows the Nyquist plots of the $FASnI_3$ solar cells at 0 V bias in the dark. The corresponding equivalent circuit of the devices is shown in Figure S7a, including the series resistance (R_s), transfer resistance (R_{tr}), recombination resistance (R_{rec}), and chemical capacitance (C).[30−32] R_s can be estimated from the high-frequency intercept on the real axis. The R_{rec} at low frequency and R_{tr} at high frequency can be assigned to the recombination at the perovskite/ETL interface and the charge transfer at the HTM/perovskite interface, respectively.[31] The Nyquist plots in Figure 4d show a main semicircle at low frequency. This main semicircle can be primarily attributed to the R_{rec} and C. We also measured the Nyquist plots of the $FASnI_3$ perovskite solar cells under different bias voltage in the dark. The corresponding fitted R_{rec} values of the TiO_2−ZnS-based cell are much higher than those of the neat TiO_2 ones, as shown in Figure S7b. These results indicate that the solar cells using the TiO_2−ZnS cascade structure have a much lower interfacial recombination rate than the neat TiO_2-based cells, as the recombination rate is inversely proportional to R_{rec}. Therefore, the ZnS surface coating on mesoporous TiO_2 effectively inhibits the recombination of charge carriers and improves cell performance.

Figure 5a shows the best-performing $FASnI_3$ perovskite solar cell built on mesoporous TiO_2−ZnS substrate, measured under reverse and forward voltage scanning. This solar cell achieved a PCE of 5.27% with a V_{oc} of 0.380 V, a J_{sc} of 23.09 mA cm^{-2}, and a FF of 60.01% when measured under reverse voltage scanning and a PCE of 4.90% with a V_{oc} of 0.373 V, a J_{sc} of 22.98 mA cm^{-2}, and a FF of 57.14% when measured under forward voltage scanning, showing a small hysteresis. Figure 5b shows the measured EQE spectrum of the solar cell using mesoporous TiO_2−ZnS, showing a high average value in the

DOI: 10.1021/jacs.6b08790
J. Am. Chem. Soc. 2016, 138, 14998−15003

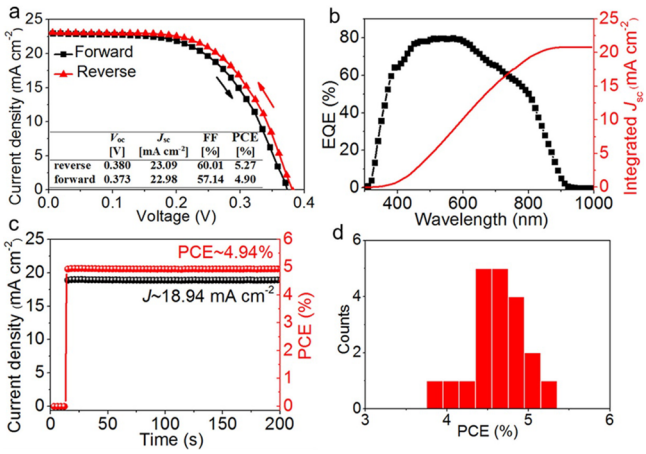

Figure 5. (a) $J-V$ curves of the best-performing $FASnI_3$ solar cell using mesoporous TiO_2–ZnS measured under reverse and forward voltage scanning. (b) EQE and integrated J_{sc} measured from the $FASnI_3$ solar cell using mesoporous TiO_2–ZnS. (c) Steady-state efficiency of the $FASnI_3$ solar cell using mesoporous TiO_2–ZnS at a constant bias voltage of 0.261 V. (d) Histograms of PCEs for 20 $FASnI_3$ solar cells using mesoporous TiO_2–ZnS measured under reverse voltage scanning.

300–900 nm wavelength range. The integrated J_{sc} calculated from the EQE curve is 20.7 mA cm^{-2}, comparable to the J_{sc} obtained from the $J-V$ measurements. The small difference arises from the fact that the EQE curve was taken at a weaker light intensity compared to the $J-V$ curves, which were measured under AM1.5G simulated irradiation.[17] The TiO_2–ZnS-based device also achieved a steady-state efficiency of 4.94%, with a steady-state current density of 18.94 mA cm^{-2} at a constant bias voltage of 0.261 V (Figure 5c). Figure 5d shows the histograms of PCEs for 20 $FASnI_3$ solar cells using mesoporous TiO_2–ZnS substrates. The average V_{oc}, J_{sc}, FF, and PCE are 0.370 ± 0.009 V, 22.35 ± 0.69 mA cm^{-2}, 56.25 ± 2.24%, and 4.65 ± 0.32%, respectively, proving a good reproducibility and high average performance of our $FASnI_3$ perovskite solar cells. We also fabricated these solar cells using the conventional one-step method[14] for comparison (Figure S8). Devices prepared by the one-step method only achieved a PCE of 2.47% with a V_{oc} of 0.262 V, a J_{sc} of 20.40 mA cm^{-2}, and a FF of 46.31% when measured under reverse voltage scanning. The low performance can be mainly attributed to poor film coverage of the $FASnI_3$ absorber.

Finally, we examined another cascade-structured ETL by using cadmium sulfide (CdS) instead of ZnS. CdS has semiconductor properties similar to those of ZnS and has been used as an interface layer to promote electron transfer and reduce charge recombination in lead-based perovskite solar cells.[33,34] The CdS films were also prepared by the SILAR method. Figure S9a shows the transmittance of the FTO/TiO_2 substrate without and with CdS film. CdS, with a relatively narrow band gap of around 2.35 eV, reduces the transmittance of the substrate in the wavelength range of 350–500 nm. Therefore, the CdS film reduces the absorption of $FASnI_3$ perovskite absorber and is thus detrimental to the device's J_{sc} output. Figure S9b shows the $J-V$ curves of the $FASnI_3$ solar cell using mesoporous TiO_2 with and without CdS. The $FASnI_3$ solar cell using mesoporous TiO_2–CdS achieved a PCE of 3.76% with a higher V_{oc} of 0.328 V, a lower J_{sc} of 22.02 mA cm^{-2}, and a FF of 52.11% when measured under reverse voltage scanning. Similar to the ZnS film, the CdS film also improves the V_{oc} of the $FASnI_3$ solar cell, thus validating our general strategy for V_{oc} improvement. From the toxicity point of view, ZnS is no doubt a better candidate than CdS, making it more suitable for incorporation in such solar cells. We should mention, however, that the V_{oc} and efficiency of the $FASnI_3$ perovskite solar cells, even with the improvement of the ZnS interface layers, are still far lower than those of Pb-based perovskite solar cells. Although the performance of tin-based perovskite cells is significantly lower, to date, than that of the Pb-based cells, the intrinsic properties of the tin perovskites and lead perovskites are comparable (e.g., band gap, details of electronic structure, etc. are similar). This suggests that, once proper conditions are found for the optimal design of the solar cells, the tin-based devices are expected to reach performance efficiencies comparable to those of the lead-based devices. In our device structure, we have to use mesoporous TiO_2 as an ETL scaffold, which is a barrier for improving the performance of the $FASnI_3$ solar cells. Further V_{oc} and efficiency enhancements are expected from the replacement/elimination of mesoporous TiO_2 and planar Sn-based perovskite devices.

CONCLUSIONS

We have shown that coating mesoporous TiO_2 with a thin ZnS layer to form a cascade structure can significantly improve the V_{oc} and PCE of the $FASnI_3$ perovskite solar cells. The best-performing $FASnI_3$ solar cell built upon a mesoporous TiO_2–ZnS scaffold achieved a PCE of 5.27% with a V_{oc} of 0.380 V, a J_{sc} of 23.09 mA cm^{-2}, and a FF of 60.01% when measured under reverse voltage scanning, which is significantly better than the reference solar cell using neat TiO_2. The enhancement in V_{oc} and subsequently PCE is mainly attributed to the ZnS interface layer effectively reducing the interfacial recombination while simultaneously facilitating the electron transfer, confirmed by both optical (PL) and electrical (EIS) measurements. Our results demonstrate that optimization of the electron transport layer, such as having a cascade structure, will be essential in pushing the efficiency of Sn-based perovskite solar cells higher.

ASSOCIATED CONTENT

Supporting Information

The Supporting Information is available free of charge on the ACS Publications website at DOI: 10.1021/jacs.6b08790.

XPS of TiO_2–ZnS, band gap and VBM of perovskite, and additional figures showing photovoltaic data and $J-V$ curves (PDF)

AUTHOR INFORMATION

Corresponding Author

*m-kanatzidis@northwestern.edu

Notes

The authors declare no competing financial interest.

ACKNOWLEDGMENTS

This work was supported in part by the ANSER Center, an Energy Frontier Research Center funded by the U.S. Department of Energy, Office of Science, and Office of Basic Energy Sciences under Award DE-SC0001059. This work made use of the EPIC facility (NUANCE Center-Northwestern University), which has received support from the MRSEC program (NSF DMR-1121262) at the Materials Research

DOI: 10.1021/jacs.6b08790
J. Am. Chem. Soc. 2016, 138, 14998–15003

Center, and the Nanoscale Science and Engineering Center (EEC-0118025/003), both programs of the National Science Foundation; the State of Illinois; and Northwestern University. The authors acknowledge Mr. Takuma Uryu (Hitachi High Technologies America, Inc.) and Mr. John Villalovos (RKI Instruments, Inc.) for performing PESA measurement and Dr. Yoshiyuki Nakajima (Riken Keiki Co. Ltd.) for fruitful discussion on the PESA results. The authors thank Takamichi Yokoyama and Duyen H. Cao for the discussion of the results.

REFERENCES

(1) Mitzi, D. B. *Prog. Inorg. Chem.* **1999**, *48*, 1.
(2) Stranks, S. D.; Eperon, G. E.; Grancini, G.; Menelaou, C.; Alcocer, M. J.; Leijtens, T.; Herz, L. M.; Petrozza, A.; Snaith, H. J. *Science* **2013**, *342*, 341.
(3) Yin, W. J.; Shi, T.; Yan, Y. *Adv. Mater.* **2014**, *26*, 4653.
(4) Yin, W.-J.; Shi, T.; Yan, Y. *J. Phys. Chem. C* **2015**, *119*, 5253.
(5) National Renewable Energy Laboratory. Best Research-Cell Efficiencies, www.nrel.gov/ncpv/images/efficiency_chart.jpg.
(6) Kazim, S.; Nazeeruddin, M. K.; Gratzel, M.; Ahmad, S. *Angew. Chem., Int. Ed.* **2014**, *53*, 2812.
(7) Saparov, B.; Mitzi, D. B. *Chem. Rev.* **2016**, *116*, 4558.
(8) Stoumpos, C. C.; Malliakas, C. D.; Kanatzidis, M. G. *Inorg. Chem.* **2013**, *52*, 9019.
(9) Mitzi, D. B.; Feild, C.; Schlesinger, Z.; Laibowitz, R. *J. Solid State Chem.* **1995**, *114*, 159.
(10) Umari, P.; Mosconi, E.; De Angelis, F. *Sci. Rep.* **2014**, *4*, 4467.
(11) Kumar, M. H.; Dharani, S.; Leong, W. L.; Boix, P. P.; Prabhakar, R. R.; Baikie, T.; Shi, C.; Ding, H.; Ramesh, R.; Asta, M.; Graetzel, M.; Mhaisalkar, S. G.; Mathews, N. *Adv. Mater.* **2014**, *26*, 7122.
(12) Hao, F.; Stoumpos, C. C.; Cao, D. H.; Chang, R. P. H.; Kanatzidis, M. G. *Nat. Photonics* **2014**, *8*, 489.
(13) Noel, N. K.; Stranks, S. D.; Abate, A.; Wehrenfennig, C.; Guarnera, S.; Haghighirad, A.-A.; Sadhanala, A.; Eperon, G. E.; Pathak, S. K.; Johnston, M. B.; Petrozza, A.; Herz, L. M.; Snaith, H. J. *Energy Environ. Sci.* **2014**, *7*, 3061.
(14) Koh, T. M.; Krishnamoorthy, T.; Yantara, N.; Shi, C.; Leong, W. L.; Boix, P. P.; Grimsdale, A. C.; Mhaisalkar, S. G.; Mathews, N. *J. Mater. Chem. A* **2015**, *3*, 14996.
(15) Hao, F.; Stoumpos, C. C.; Guo, P.; Zhou, N.; Marks, T. J.; Chang, R. P.; Kanatzidis, M. G. *J. Am. Chem. Soc.* **2015**, *137*, 11445.
(16) Zhang, M.; Lyu, M.; Yun, J.-H.; Noori, M.; Zhou, X.; Cooling, N. A.; Wang, Q.; Yu, H.; Dastoor, P. C.; Wang, L. *Nano Res.* **2016**, *9*, 1570.
(17) Yokoyama, T.; Cao, D. H.; Stoumpos, C. C.; Song, T. B.; Sato, Y.; Aramaki, S.; Kanatzidis, M. G. *J. Phys. Chem. Lett.* **2016**, *7*, 776.
(18) Sabba, D.; Mulmudi, H. K.; Prabhakar, R. R.; Krishnamoorthy, T.; Baikie, T.; Boix, P. P.; Mhaisalkar, S.; Mathews, N. *J. Phys. Chem. C* **2015**, *119*, 1763.
(19) Lee, S. J.; Shin, S. S.; Kim, Y. C.; Kim, D.; Ahn, T. K.; Noh, J. H.; Seo, J.; Seok, S. I. *J. Am. Chem. Soc.* **2016**, *138*, 3974.
(20) Ongul, F.; Ulutas, U.; Yuksel, S. A.; Yesilkaya, S. S.; Gunes, S. *Synth. Met.* **2016**, *220*, 1.
(21) Xu, G.; Ji, S.; Miao, C.; Liu, G.; Ye, C. *J. Mater. Chem.* **2012**, *22*, 4890.
(22) Bredol, M.; Matras, K.; Szatkowski, A.; Sanetra, J.; Prodi-Schwab, A. *Sol. Energy Mater. Sol. Cells* **2009**, *93*, 662.
(23) Ke, W.; Fang, G.; Lei, H.; Qin, P.; Tao, H.; Zeng, W.; Wang, J.; Zhao, X. *J. Power Sources* **2014**, *248*, 809.
(24) Cao, D. H.; Stoumpos, C. C.; Farha, O. K.; Hupp, J. T.; Kanatzidis, M. G. *J. Am. Chem. Soc.* **2015**, *137*, 7843.
(25) Yang, M.; Zhou, Y.; Zeng, Y.; Jiang, C. S.; Padture, N. P.; Zhu, K. *Adv. Mater.* **2015**, *27*, 6363.
(26) Jeon, N. J.; Noh, J. H.; Kim, Y. C.; Yang, W. S.; Ryu, S.; Seok, S. I. *Nat. Mater.* **2014**, *13*, 897.
(27) Ahn, N.; Son, D. Y.; Jang, I. H.; Kang, S. M.; Choi, M.; Park, N. G. *J. Am. Chem. Soc.* **2015**, *137*, 8696.
(28) Ke, W.; Xiao, C.; Wang, C.; Saparov, B.; Duan, H. S.; Zhao, D.; Xiao, Z.; Schulz, P.; Harvey, S. P.; Liao, W.; Meng, W.; Yu, Y.; Cimaroli, A. J.; Jiang, C. S.; Zhu, K.; Al-Jassim, M.; Fang, G.; Mitzi, D. B.; Yan, Y. *Adv. Mater.* **2016**, *28*, 5214.
(29) Chung, I.; Lee, B.; He, J.; Chang, R. P.; Kanatzidis, M. G. *Nature* **2012**, *485*, 486.
(30) Chandiran, A. K.; Yella, A.; Mayer, M. T.; Gao, P.; Nazeeruddin, M. K.; Gratzel, M. *Adv. Mater.* **2014**, *26*, 4309.
(31) Wang, K.; Shi, Y.; Li, B.; Zhao, L.; Wang, W.; Wang, X.; Bai, X.; Wang, S.; Hao, C.; Ma, T. *Adv. Mater.* **2016**, *28*, 1891.
(32) Ke, W.; Fang, G.; Wang, J.; Qin, P.; Tao, H.; Lei, H.; Liu, Q.; Dai, X.; Zhao, X. *ACS Appl. Mater. Interfaces* **2014**, *6*, 15959.
(33) Liu, J.; Gao, C.; Luo, L.; Ye, Q.; He, X.; Ouyang, L.; Guo, X.; Zhuang, D.; Liao, C.; Mei, J.; Lau, W. *J. Mater. Chem. A* **2015**, *3*, 11750.
(34) Liu, C.; Qiu, Z.; Meng, W.; Chen, J.; Qi, J.; Dong, C.; Wang, M. *Nano Energy* **2015**, *12*, 59.

DOI: 10.1021/jacs.6b08790
J. Am. Chem. Soc. 2016, 138, 14998−15003